MIT Libraries | DSpace@MIT

MIT Open Access Articles

Quantum Imaging by Coherent Enhancement

The MIT Faculty has made this article openly available. ***Please share*** how this access benefits you. Your story matters.

Citation: Low, Guang Hao, Theodore J. Yoder, and Isaac L. Chuang. "Quantum Imaging by Coherent Enhancement." Physical Review Letters 114.10 (2015). © 2015 American Physical Society

As Published: http://dx.doi.org/10.1103/PhysRevLett.114.100801

Publisher: American Physical Society

Persistent URL: http://hdl.handle.net/1721.1/95994

Version: Final published version: final published article, as it appeared in a journal, conference proceedings, or other formally published context

Terms of Use: Article is made available in accordance with the publisher's policy and may be subject to US copyright law. Please refer to the publisher's site for terms of use.

Massachusetts Institute of Technology

Quantum Imaging by Coherent Enhancement

Guang Hao Low, Theodore J. Yoder, and Isaac L. Chuang
Center for Ultracold Atoms, Research Laboratory of Electronics, and Department of Physics, Massachusetts Institute of Technology, Cambridge, Massachusetts 02139, USA
(Received 29 September 2014; published 11 March 2015)

Conventional wisdom dictates that to image the position of fluorescent atoms or molecules, one should stimulate as much emission and collect as many photons as possible. That is, in this classical case, it has always been assumed that the coherence time of the system should be made short, and that the statistical scaling $\sim 1/\sqrt{t}$ defines the resolution limit for imaging time t. However, here we show in contrast that given the same resources, a long coherence time permits a higher resolution image. In this quantum regime, we give a procedure for determining the position of a single two-level system and demonstrate that the standard errors of our position estimates scale at the Heisenberg limit as $\sim 1/t$, a quadratic, and notably optimal, improvement over the classical case.

DOI: 10.1103/PhysRevLett.114.100801 PACS numbers: 06.20.-f, 03.67.-a, 06.30.Bp, 42.50.-p

Precisely imaging the location of one or more point objects is a problem ubiquitous in science and technology. While the resolution of an image is typically defined through the diffraction limit as the wavelength $\sim\lambda$ of illuminating light, the final estimate of object position instead exhibits a shot-noise limited standard deviation σ that scales with the number of scattered photons detected—a consequence of the law of large numbers. Thus, in the absence of environmental noise, it is the time allowed for accumulating statistics that appears to limit precise position measurements.

Surprisingly, when the objects to be imaged are imbued with quantum properties, these well-known classical limits on resolution and standard deviation can be improved. Impressive suboptical resolutions of $\sim\lambda/10$ [1,2] are obtainable by advanced microscopy [2] protocols such as STED [3], RESOLFT [4], STORM [5], and PALM [6]. Each, in its own way, exploits the coherence of a quantum object by storing its position x_i in its quantum state $|\psi\rangle$ over an extended period of time. However, even for state of the art, it is still the statistical scaling $\sigma \sim 1/\sqrt{t}$ that limits a position estimate taking time t.

Yet, fundamentally, coherent quantum objects allow for a standard deviation scaling quadratically better, as $\sigma \sim 1/t$. This so-called Heisenberg limit [7] is a fundamental restriction of nature that bounds the standard deviation of a single-shot phase estimate of $|\psi\rangle$, i.e., given a single copy of $|\psi\rangle$, to $\sim 1/t$, a bound attainable in the regime of long coherence [8–10].

How then can quantum coherence be fully exploited to estimate a quantum object's position? An apparent contradiction arises since photon scattering rates approach zero in the limit of infinite coherence, in contrast to traditional imaging, where maximizing scattering is desirable. A similar problem arises in magnetic resonance imaging, but is there resolved by a two-step process: map x_i coherently to $|\psi\rangle$, then readout $|\psi\rangle$ using just a few photons. However, current approaches have two flaws. First, the mapping is typically ambiguous [Fig. 1(a)]. Because of the periodicity of quantum phases, multiple x_i can be encoded into the same observable of $|\psi\rangle$—often the transition probability $s(x_i)$. Second, the mapping resolution r—the length scale over which $s(x_i)$ varies—cannot be improved arbitrarily in an effective manner. Doing so, with say a long sequence of L coherent excitations, either introduces more ambiguity or requires time that does not perform better than the statistical scaling [Fig. 1(b)]. Approaches that estimate position with Heisenberg-limited scaling must overcome these two challenges.

Such well-known difficulties are apparent when using a spatially varying coherent drive, e.g., a Gaussian beam, that produces excitations varying over space $\sim\lambda$. Because of projection noise [11], $s(x_i)$ can only be estimated with error

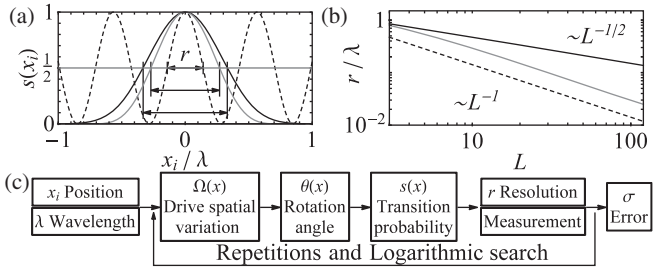

FIG. 1. (a) Map from position x_i to transition probability $s(x_i)$. This is ideally unambiguous with a single narrow peak of width r (thin; thick lines). The ambiguous map has multiple peaks (dashed line). (b) Scaling of r with the number of coherent drive pulses L. The optimal scaling is $\sim 1/L$ (dashed; thin lines), but often suboptimal $\sim 1/\sqrt{L}$ for unambiguous maps (thick line). (c) Procedure outline for estimating x_i with error σ scaling at the Heisenberg limit. This combines an optimal r-scaling unambiguous map with measurement in a logarithmic search.

 © 2015 American Physical Society

scaling $\sim 1/\sqrt{t}$. Thus, for any given r, a standard deviation $\sigma \sim r/\sqrt{t}$ results. Working around projection noise and improving these resolutions is the focus of much work in magnetic resonance as well as quantum information science with trapped ions [12–17]. Unfortunately, state-of-the-art [13,18,19] excitation sequences, or pulse sequences, that produce a single unambiguous peak are suboptimal—they offer a resolution of $r \sim \lambda/\sqrt{L}$ (Fig. 1), no better than the statistical scaling.

We present a new procedure that images quantum objects with standard deviation $\sigma \sim 1/t$, using a two-step imaging process which unambiguously maps spatial position to quantum state, allowing for readout with imaging resolution that scales as the optimum achievable by the Heisenberg limit. Like prior art, a pulse sequence is employed to implement the unambiguous mapping. In contrast, though, we develop new sequences with the optimum resolution scaling $r \sim 1/L$ (Fig. 1). Because of the narrowness of r, measuring the quantum state is much more likely to tell one where the object is not, rather than where it is located. Thus, our optimal unambiguous mapping alone is insufficient for achieving $\sigma \sim 1/t$. This issue is resolved using a logarithmic search, modeled after quantum phase estimation [8–10], that applies our mapping several times with varying resolutions. This logical flow [Fig. 1(c)] leads to an imaging algorithm with optimal scaling $\sigma \sim 1/t$. From the classical perspective that imaging should be done with short coherence times and maximal photon scattering, our algorithm is a complete surprise. In fact, our results imply that the best method for imaging quantum objects is to collect very few photons from a source that can be coherently controlled.

We begin by defining the resources required for imaging the position of a quantum object in one dimension. The action of pulse sequences on this system is briefly reviewed to demonstrate the mapping of spatial position to transition probability. This allows us to define the unambiguity and optimality criteria for a transition probability. We show that our new pulse sequences have both properties. These properties enable an efficient logarithmic search for system position, solving the projection noise issue. We then discuss estimates of real-world performance, generalizations to higher dimensions, and multiple objects.

Consider a quantum two-level system in state $|\psi\rangle$ at an unknown position x_i contained in a known interval I of width $\lesssim\lambda$. Measurements in the $\{|0\rangle, |1\rangle\}$ basis are assumed. Provided is a coherent drive, over which we have phase ϕ and duration τ control, with a known spatially varying Rabi frequency $\Omega(x)$, where $x = x_i - x_c$ can be translated by arbitrary distance x_c. With this coherent drive, a unitary rotation $U_\phi[\theta] = e^{-i(\theta/2)[\cos(\phi)\hat{X}+\sin(\phi)\hat{Y}]}$, where $\hat{X}$, $\hat{Y}$ are Pauli matrices, that traverses angle $\theta(x) = \Omega(x)\tau$ can be applied. Combined with measurements, this allows us to prepare $|0\rangle$ by repeated projection. Chaining L such discrete rotations generates a pulse sequence $\mathcal{S} = U_{\phi_L}[\theta], \ldots, U_{\phi_1}[\theta] \equiv (\phi_1, .., \phi_L)$. When applied to $|0\rangle$, this results in the state $\mathcal{S}|0\rangle$ and the transition probability $p(\theta) = |\langle 1|\mathcal{S}|0\rangle|^2$ in θ coordinates. As θ depends on position x_i, a map from spatial coordinates to transition probability is achieved through $s(x) = p(\theta(x))$.

The criteria of unambiguity and optimality can be expressed as four constraints on the form of $s(x)$. Unambiguity means that $s(x)$ has only a single sharp peak of width r within interval I, so that excitation with high probability only occurs in a small contiguous space. As $p(\theta)$ is periodic in $\theta \to \theta \pm 2\pi$ and, for odd L, necessarily peaks at $p(\theta = \pi) = 1$, one finds the following three constraints sufficient to guarantee unambiguity: (1) $\theta(x)$ varies monotonically with x, (2) $0 \le \theta(x) < 2\pi$, and (3) $p(\theta)$ is bounded by some $\delta_r^2 \ll 1$ outside of the $\theta = \pi$ peak. Optimality is defined as resolution scaling at the Heisenberg limit. So, the last constraint is (4) $r \sim 1/L$.

Constraints (1) and (2) relate to the spatial variation of $\Omega(x)$ and are easily satisfied. One practical realization is a Gaussian diffraction-limited beam with spatial profile $\Omega(x) = \Omega_0 e^{-x^2/4\lambda^2}$, restricted to $x > 0$, so that $\theta(x)$ is monotonic in x. By choosing $0 < \tau < 2\pi/\Omega_0$, $\theta(x)$ falls in the desired principle range. In particular, the choice $\tau = \sqrt{e}\pi/\Omega_0$ minimizes r as the necessary peak in $s(x)$ occurs at $x_\pi = \sqrt{2}\lambda$, where $\theta(x_\pi) = \pi$ and the gradient $\theta' = \max_x|d\theta(x)/dx|$ is also steepest. This allows us to define the resolution $\theta_r = r\theta'/2$ in θ coordinates.

Constraints (3) and (4) relate to $p(\theta)$ and are satisfied by our new family of pulse sequences $\mathcal{S}_L$, which realize

$$\begin{aligned} p_L(\theta;\delta_r) &= |T_L[\beta_L(\delta_r)\sin(\theta/2)]/T_L[\beta_L(\delta_r)]|^2, \\ \theta_r(L) &= 2\mathrm{sech}^{-1}(\delta_r)/L + \mathcal{O}(1/L^3), \\ r &= 2\theta_r(L)/\theta', \end{aligned} \tag{1}$$

plotted in Fig. 2, where $T_L[x] = \cos[L\cos^{-1}(x)]$ is the Lth Chebyshev polynomial and $\beta_L(x) = T_{L^{-1}}[x^{-1}]$. Primary features of $p_L(\theta;\delta_r)$ include an optimally narrow, like $\theta_r \sim 1/L$, central peak given a uniform bound δ_r^2 on sidelobes [20]. We find it useful to define the half-width θ_a at arbitrary heights $\delta_a^2 > \delta_r^2$ (Fig. 2):

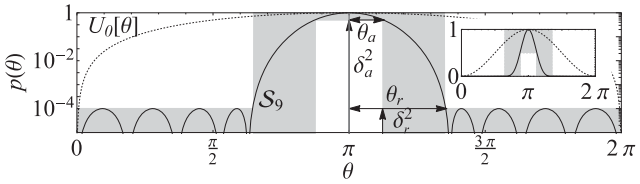

FIG. 2. Transition probability $p(\theta)$ of the sequence $\mathcal{S}_L$ (solid line) plotted for $L = 9$ in comparison to a single rotation $U_0[\theta]$ (dotted line). The range of the envelope $p(\theta;\theta_r,\theta_a)$ is shaded. Primary features of $\mathcal{S}_L$ are sidelobes of uniform bounded error δ_r^2 and a central peak with width parameters θ_r, θ_a that scale as $\sim 1/L$. The inset plots the same on a linear scale.

$$\theta_a(L)=\theta_r(L)R,$$
$$R=\sqrt{1-[\mathrm{sech}^{-1}(\delta_r/\delta_a)/\mathrm{sech}^{-1}(\delta_r)]^2}+\mathcal{O}(1/L^2). \tag{2}$$

The phases that implement arbitrarily long $\mathcal{S}_L$ are elegantly described in closed form. We first consider the broadband variant $\mathcal{S}_L^B=(\chi_1,\ldots,\chi_L)$, which realizes $p_L^B(\theta;\delta_r)=1-p_L(\theta-\pi;\delta_r)$ and is related to $\mathcal{S}_L$ via $\phi_k=(-1)^k\chi_k+2\sum_{h=1}^{k-1}(-1)^h\chi_h$ [21]. It is easily verified that $\mathcal{S}_3^B=(\chi,0,\chi)$ has $\chi=2\tan^{-1}[\tan(\pi/3)\sqrt{1-\beta_3^{-2}(\delta_r)}]$. As $(\chi,0,\chi)$ is symmetric [18,19], $\mathcal{S}_3^B$ implements an effective rotation of angle θ_e, defined through $1-p_L^B(\theta;\delta_r)=\cos^2(\theta_e/2)$, about some axis in the $\hat{x}$-$\hat{y}$ plane. Thus, replacing each base pulse in $\mathcal{S}_{L_2=3}^B[\delta_r]$ with a different sequence $\mathcal{S}_{L_1=3}^B[1/\beta_{L_2}(\delta_r)]$ produces the transition profile $p_{L_1L_2}^B(\theta;\delta_r)$ by repeatedly applying the semigroup property $T_n[T_m[x]]=T_{\mathrm{nm}}[x]$ of Chebyshev polynomials. For $L_2=3$ and any odd L_1, this corresponds exactly to the transition profile of $\mathcal{S}_{3L_1}^B[\delta_r]=(\chi,0,\chi)\circ\mathcal{S}_{L_1}^B[1/\beta_3(\delta_r)]$, where $\circ$ defines a nesting operator $(a_1,a_2,\ldots)\circ(b_1,b_2,\ldots)=(a_1+b_1, a_1+b_2,\ldots,a_2+b_1,a_2+b_2,\ldots)$. As we provide $L_1=3$, by induction the phases of $\mathcal{S}_{3^n}^B[\delta_r]$ and $\mathcal{S}_{3^n}[\delta_r]$ can be obtained in closed form as a function of δ_r for all $n\in\mathbb{Z}^+$.

After $\mathcal{S}_L$ is applied to $|0\rangle$ for some choice of beam position x_c, measuring the state of the system extracts encoded positional information. As visualized with the envelope in Fig. 2:

$$p(\theta;\theta_r,\theta_a)=\begin{cases}\geq\delta_a^2 & |\theta-\pi|\leq\theta_a\\ \in[0,1] & \theta_a<|\theta-\pi|<\theta_r\\ \leq\delta_r^2 & \text{otherwise,}\end{cases} \tag{3}$$

if $|1\rangle$ is obtained after a measurement, the object is located with high probability in the central peak. Thus, we assign the estimated object position x_e to a spatial interval Δ^r of width $r=2\theta_r(L)/\theta'$ centered on x_c+x_π. Conversely, if $|0\rangle$ is obtained, the x_e is located outside, in $I\backslash\Delta^a$, with high probability, where Δ^a is centered on x_c+x_π with width $2\theta_a/\theta'$. However, projection noise means that false positives or negatives can occur. Fortunately, these can be made exponentially improbable by taking l repeats.

The probability P of an incorrect classification, that is, assigning x_e to an interval that does not contain x_i, is straightforward. Over l repetitions, we measure $|1\rangle$ k times. Note that k is drawn from a binomial distribution of l trials with mean $\bar{k}$. If $k/l\geq\bar{p}=(\delta_a^2+\delta_r^2)/2$, we assign $x_e\in\Delta^r$. Otherwise, we assign $x_e\in I\backslash\Delta^a$. Thus,

$$\begin{aligned}P&=\max(P_1,P_2)\leq\exp[-l(\delta_a^2-\delta_r^2)^2/2],\\ P_1&=\Pr[x_e\in I\backslash\Delta^a|x_i\in\Delta^a]\leq\Pr[k<l\bar{p}|\bar{k}=l\delta_a^2],\\ P_2&=\Pr[x_e\in\Delta^r|x_i\in I\backslash\Delta^r]\leq\Pr[k\geq l\bar{p}|\bar{k}=l\delta_r^2],\end{aligned} \tag{4}$$

where P bounded by Hoeffding's inequality applied to binomial distributions [22] illustrates its exponential decay with l—an exact evaluation of the cumulative probability improves this significantly. Thus, x_e can be reliably classified to either inside or outside a region of width $\sim1/L$ in ~1 measurements with $P\ll1$.

A key insight allows us to sidestep the $\sigma\sim1/\sqrt{t}$ scaling of projection noise. Once the object has been classified to Δ^r by $\mathcal{S}_L$, subintervals of width K times narrower than Δ^r can be queried by $\mathcal{S}_{KL}$. As the width of these subintervals scales optimally like $\sim1/L$, it is never profitable, in the coherent regime, to accumulate statistics indefinitely. Rather, L should be increased in geometric progression as far as coherence times allow. In other words, imaging proceeds by logarithmic search, illustrated in Fig. 3, where in the nth iteration, x_e has been classified to the region I_n of width $r_n=2\theta_r(L_n)/\theta'$ with a length $L_n=L_0K^n$ sequence. Although conceptually similar to a binary search, we must account for two key differences: (1) queries are corrupted by projection noise and (2) the classification intervals are asymmetric, i.e., $\Delta^r\neq\Delta^a$.

The search is initialized by choosing the largest L_0 such that r_0 exceeds the initial width of I. This is then followed by $n=1,\ldots,M$ iterations of a recursive process. The nth iteration involves three steps. First, I_{n-1} is split into $\lceil K/R\rceil$ smaller subintervals of equal width, each centered on x_d, where $d=1,\ldots,\lceil K/R\rceil$, $K\in\mathbb{Z}^+$, and the choice of δ_a^2 determines R in Eq. (2). Second, the classification procedure involving l applications of $\mathcal{S}_{L_n}$ is then applied for each d with shifted beam center $x_c=x_d-x_\pi$ until for some d a classification into Δ^r occurs. Third, we update $I_n=\Delta^r$, which is of width $r_n=r_{n-1}/K$. By induction over M iterations, x_e lies in an interval width $r_M=r_0/K^M$. Since $K>1$, exponential precision is achieved in only a linear number of $\sim M$ state initializations and measurements. Any misclassification of $x_e\in\Delta^r$ such that $x_i\notin\Delta^r$ will be detected in the next iteration as the probability of misclassifying $x_e\in\Delta^r$ again becomes vanishingly small like $\mathcal{O}(P^2)$. In that case, the previous iteration is repeated.

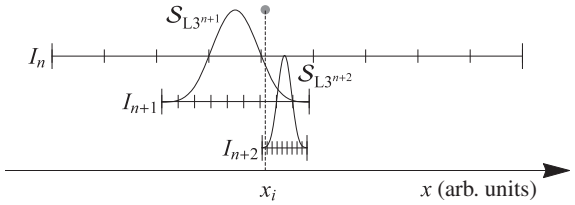

FIG. 3. The logarithmic search illustrated for an object located at x_i. At the nth iteration, the estimate has been assigned to the interval $x_e\in I_n$. I_n is split into $\lceil K/R\rceil$ subintervals, and the classification procedure with $\mathcal{S}_{L_0K^{n+1}}$ is applied to each subinterval. The first positive classification to Δ^r further narrows the estimate to $x_e\in\Delta^r=I_{n+1}$. In this example, $K=3$, $R\approx1/3$, $\delta_a^2=1/2$, $\delta_r^2=10^{-4}$.

Assuming $x_i \in I_M$ is uniformly distributed, the standard deviation is $\sigma \approx (r_M/\sqrt{12})[1+\mathcal{O}(P)]$.

The run time $t = \tau E \sum_{n=1}^{M} L_n$ of this logarithmic search is a geometric sum over M iterations, each involving an expected number $E = \lceil K/R \rceil l/2 + \mathcal{O}(P)$ applications of $\mathcal{S}_{L_n}$. Letting $\Omega' = |d\Omega(x)/dx|_{x=x_\pi}$, we have

$$t = E\frac{\tau L_0(K^M-1)}{K-1} \approx \frac{2E\,\mathrm{sech}^{-1}(\delta_r)}{\sqrt{3}(K-1)}\frac{1}{\Omega'\sigma}, \tag{5}$$

where we have used $K^M \gg 1$, $K^M = r_0/r_M$, $r_0\tau \approx 2\theta_r(L_0)/\Omega'$, and $r_M \approx \sqrt{12}\sigma$. We arrive at our final result: an estimate of object position x_e with standard deviation $\sigma \sim 1/\Omega' t$ exhibiting a Heisenberg-limited scaling with time, and requiring $M \sim \log(1/\sigma)$ measurements. Inserting $K=3$, $l=5$, $\delta_r^2 = \frac{7}{20}$, $\delta_a^2 = \frac{13}{20}$ into Eq. (5), evaluating E to $\mathcal{O}(P^2)$, and Eq. (4) exactly gives $t \approx 26/\Omega'\sigma$. This compares favorably to the ultimate lower bound of $t \geq \pi/\Omega'\sigma$, which we obtain by combining the identity $\theta = \Omega\tau$ with optimal schemes of phase estimation for θ in related systems [9] wherein entanglement between trials and nonlocal measurements are allowed—resources which are extreme experimental challenges.

Notably, our imaging procedure gracefully degrades in the presence of noise found in real systems. Noise replaces $\mathcal{S}$ and $|0\rangle$ with an implementation-dependent quantum channel $\mathcal{E}(\rho)$ and an imperfect initial state ρ_i, respectively, to produce $\rho_{\text{noise}} = \mathcal{E}(\rho_i)$, in comparison to the ideal case of $\rho_{\text{ideal}} = \mathcal{S}|0\rangle\langle 0|\mathcal{S}^\dagger$. As trace distance [8] $\mathrm{Tr}D(\rho_{\text{ideal}}, \rho_{\text{noise}}) = \gamma$ bounds the difference in measurement probabilities using any measurement basis, noise shifts the envelope in Eq. (3) by $\delta_r^2 \to \delta_r^2 + \gamma$, $\delta_a^2 \to \delta_a^2 - \gamma$ and modifies Eq. (4):

$$\begin{aligned} &P \leq \exp\left[-l(\delta_a^2 - \delta_r^2 - 2\gamma)^2/2\right] \ll 1, \\ &0 < \delta_a^2 - \delta_r^2 - 2\gamma. \end{aligned} \tag{6}$$

As long as $\gamma < \frac{1}{2}$, classification succeeds *independent* of the noise model, as we can always satisfy Eq. (6) by some choice of δ_r, δ_a, and $l(\gamma) \propto (\delta_a^2 - \delta_r^2 - 2\gamma)^{-2}$. Success for $\gamma \geq \frac{1}{2}$ depends on details of the noise model. Using the triangle inequality, we can also separate the contributions from $\mathcal{E}(\rho)$ and ρ_i to obtain $\gamma \leq \gamma_i + \gamma_n$, where $\gamma_i = \mathrm{Tr}D(|0\rangle\langle 0|, \rho_i)$ and $\gamma_n = \mathrm{Tr}D[\rho_{\text{ideal}}, \mathcal{E}(|0\rangle\langle 0|)]$. Other errors, e.g., nonideal measurement bases, can be similarly included. Of course, in any system with finite coherence time τ_c, γ increases with sequence length. To illustrate, consider a completely depolarizing channel where $\gamma_n = \frac{1}{2}(1 - e^{-tL_n/\tau_c})$ and ignore initial state errors so $\gamma_i = 0$. For fixed δ_a, δ_r, the run time in Eq. (5) becomes $t \propto \sum_{n=1}^{M} l(\gamma_n) K^n$. As the final standard deviation $\sigma \propto 1/K^M$, the instantaneous scaling in the presence of noise,

$$\frac{dt}{d(\sigma^{-1})} \propto 1 + \frac{2}{\delta_a^2 - \delta_r^2}\frac{\tau L_M}{\tau_c} + \mathcal{O}[(\tau L_M/\tau_c)^2], \tag{7}$$

degrades continuously from the noiseless Heisenberg-limited scaling $\lim_{\tau_c \to \infty}[dt/d(\sigma^{-1})] \propto 1$ to the statistical scaling $[dt/d(\sigma^{-1})] \propto \sqrt{t}$. In the regime of strong decoherence at $\tau L_M \sim \tau_c$, accumulating statistics with $\mathcal{S}_{L_M}$ and applying the law of large numbers becomes more time efficient than a logarithmic search.

Generalizations of our imaging procedure are possible. For example, finding the (x_i, y_i, z_i) coordinates of an object in three dimensions is reducible to three separate one-dimensional problems by using three cylindrical Gaussian beams oriented about orthogonal axes with spatial profiles $\theta(x,y,z) = \sqrt{e}\pi e^{-s^2/4\lambda^2}$, $s \in \{x,y,z\}$. More sophisticated methods include the use of radial Gaussian beams $\theta(x,y) = \sqrt{e}\pi e^{-(x^2+y^2)/4\lambda^2}$ to triangulate the object position in two dimensions. Additionally, with multiple objects, cross talk can be suppressed by decreasing δ_r^2 by a factor linearly proportional to the number of objects. This allows subintervals of width σ that contain objects to still be found in $t \sim 1/\sigma$.

Many avenues of further inquiry arise from this work. For example, our pulse sequences mimic Dolph-Chebyshev window functions [20,23] studied in digital signal filtering [24,25]. This suggests a connection for applying the extensive machinery developed for signal processing to pulse sequences, interpreted as *quantum* filters [26]. In particular, variants or even generalizations of standard quantum phase estimation [8–10] can be found as done here: the sequence U_ϕ^L used in the standard scheme is a special case of our sequences $\lim_{\delta_r \to 1}\mathcal{S}_L = U_\phi^L$. One could also imbue the quantum object with additional levels or qubits, possibly leading to more robust schemes [27] that could even exploit entanglement [28]. Finally, the techniques presented apply to the entire electromagnetic spectrum. Thus, exciting possibilities include using microwaves of $\lambda \sim 1$ cm to efficiently measure nanoscale $\sim$10 nm features, or novel forms of magnetic resonance imaging where instead of using magnetic field gradients, a spatially varying radio-frequency drive strength provides nuclei or quantum dots with high-resolution positional information.

G. H. L. acknowledges support from the ARO Quantum Algorithms program. T. J. Y. acknowledges support from the NSF iQuISE IGERT program. I. L. C. acknowledges support from the NSF CUA.

[1] E. Betzig and J. K. Trautman, Science **257**, 189 (1992).
[2] S. W. Hell, Science **316**, 1153 (2007).
[3] A. S. Trifonov, J. Jaskula, C. Teulon, D. R. Glenn, N. Bar-Gill, and R. L. Walsworth, Adv. At. Mol. Opt. Phys. **62**, 279 (2013).
[4] M. Hofmann, C. Eggeling, S. Jakobs, and S. W. Hell, Proc. Natl. Acad. Sci. U.S.A. **102**, 17565 (2005).

[5] M. J. Rust, M. Bates, and X. Zhuang, Nat. Methods **3**, 793 (2006).
[6] E. Betzig, G. H. Patterson, R. Sougrat, O. W. Lindwasser, S. Olenych, J. S. Bonifacino, M. W. Davidson, J. Lippincott-Schwartz, and H. F. Hess, Science **313**, 1642 (2006).
[7] E. Demkowicz-Dobrzanski, J. Kolodynski, and M. Guta, Nat. Commun. **3**, 1063 (2012).
[8] M. A. Nielsen and I. L. Chuang, *Quantum Computation and Quantum Information* (Cambridge University Press, Cambridge, England, 2004).
[9] D. W. Berry, B. L. Higgins, S. D. Bartlett, M. W. Mitchell, G. J. Pryde, and H. M. Wiseman, Phys. Rev. A **80**, 052114 (2009).
[10] B. L. Higgins, D. Berry, S. Bartlett, M. Mitchell, H. M. Wiseman, and G. Pryde, New J. Phys. **11**, 073023 (2009).
[11] W. M. Itano, J. C. Bergquist, J. J. Bollinger, J. M. Gilligan, D. J. Heinzen, F. L. Moore, M. G. Raizen, and D. J. Wineland, Phys. Rev. A **47**, 3554 (1993).
[12] D. Wineland, C. Monroe, W. M. Itano, D. Leibfried, B. E. King, and D. M. Meekhof, J. Res. Natl. Inst. Stand. Technol. **103**, 259 (1998).
[13] N. V. Vitanov, Phys. Rev. A **84**, 065404 (2011).
[14] C. M. Shappert, J. T. Merrill, K. R. Brown, J. M. Amini, C. Volin, S. C. Doret, H. Hayden, C. S. Pai, K. R. Brown, and A. W. Harter, New J. Phys. **15**, 083053 (2013).
[15] C. Shen, Z. X. Gong, and L. M. Duan, Phys. Rev. A **88**, 052325 (2013).
[16] D. Le Sage, K. Arai, D. R. Glenn, S. J. DeVience, L. M. Pham, L. Rahn-Lee, M. D. Lukin, A. Yacoby, A. Komeili, and R. L. Walsworth, Nature (London) **496**, 486 (2013).
[17] J. T. Merrill, S. C. Doret, G. D. Vittorini, J. P. Addison, and K. R. Brown, Phys. Rev. A **90**, 040301 (2014).
[18] J. A. Jones, Phys. Rev. A **87**, 052317 (2013).
[19] G. H. Low, T. J. Yoder, and I. L. Chuang, Phys. Rev. A **89**, 022341 (2014).
[20] C. L. Dolph, Proc. IRE **34**, 335 (1946).
[21] M. H. Levitt, Prog. Nucl. Magn. Reson. Spectrosc. **18**, 61 (1986).
[22] W. Hoeffding, J. Am. Stat. Assoc. **58**, 13 (1963).
[23] F. Harris, Proc. IEEE **66**, 51 (1978).
[24] A. Fettweis, IEEE Trans. Circuit Syst. **31**, 31 (1984).
[25] A. Fettweis, Proc. IEEE **74**, 270 (1986).
[26] A. Soare, H. Ball, D. Hayes, J. Sastrawan, M. C. Jarratt, J. J. McLoughlin, X. Zhen, T. J. Green, and M. J. Biercuk, Nat. Phys. **10**, 825 (2014).
[27] J. Borregaard and A. S. Sørensen, Phys. Rev. Lett. **111**, 090802 (2013).
[28] E. M. Kessler, P. Kómár, M. Bishof, L. Jiang, A. S. Sørensen, J. Ye, and M. D. Lukin, Phys. Rev. Lett. **112**, 190403 (2014).